

A Multi-Carrier Molecular Communication Model for Astrocyte Tissues

Ligia F. Borges, Michael T. Barros, Michele Nogueira

NR2/CCSC - Federal University of Paraná, Brazil

CBIG/Biomeditech, Faculty of Medicine and Health Technology, Tampere University, Finland.

Emails: {lfborges,michele}@inf.ufpr.br, michael.barros@tuni.fi

Abstract—This paper presents a multi-carrier molecular communication model for astrocyte tissues. The model considers molecular diversity and analyses channel path loss and capacity for molecular communication based on the concentration of Inositol Triphosphate (IP_3) and calcium (Ca^{2+}) molecules. Without loss of generality, we investigate the spatiotemporal concentration of these molecules and how both intracellular and intercellular signaling dictates signal propagation inside astrocytes tissues. Astrocytes are the most abundant glial cell type in the adult brain and play essential roles in brain function, such as modulating neuronal excitation, inhibition, and synaptic transmission. Results show that the cooperation between these two molecules reduce path loss, improves data propagation, and can be an alternative for data encoding and transmission. The multi-carrier molecular communication using IP_3 and Ca^{2+} has overall superior performance, showing the potential benefits of molecular diversity.

I. INTRODUCTION

Biological systems have inspired promising approaches for engineering data communication in nanonetworks [1]. The main example is the natural signaling process of human body cells, which can exchange information based on the transmission, propagation, and reception of molecules, through biochemical and physical processes following the molecular communication (MC) paradigm. In biological cells, natural components are similar to parts of data communication systems, such as transmitters, receivers, encoding, and memory capacity, among others [2].

Since natural cells exhibit a variety of molecules and their corresponding pathways, we capitalize on the diversity of molecules and their relationships to improve performance and reliability in MC. Moreover, we advocate for molecular diversity as a leading alternative to achieve low complexity in multi-user MC systems. Hence, we use the IP_3/Ca^{2+} pathway and intercellular signaling, which has important functions for various regulatory purposes, including neuronal transmission, cell growth, and death.

Fig. 1 illustrates a molecular communication system, highlighting the paralleled Ca^{2+} and IP_3 channels, adapted from principles of multi-carrier systems. In this paper, we present a multi-carrier molecular communication model for astrocyte tissues. The model considers the diversity of molecules, where

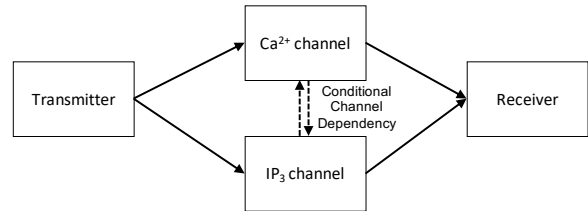


Fig. 1: The multi-carrier IP_3/Ca^{2+} signaling based MC System

each type of molecule performs the role of a channel. The model allows the analysis of the Spatio-temporal concentration of Ca^{2+} and IP_3 molecules, and how both intracellular and intercellular signaling dictates signal propagation inside astrocytes tissues considering principles of a multi-carrier system. Astrocytes are the most abundant glial cells in the central nervous system and offer different applications, *e.g.*, information processing and synaptic transmission. Astrocyte's role in neuroscience is a hot topic holding the hope of explaining neurodegenerative disease origins.

Our model represents gap junctions connecting astrocytes. When a gap junction opens, it allows cells to exchange small molecules with neighboring cells (intercellular communication) [3]. We advance the *Exact Stochastic Chemical Reaction-Diffusion* ordinary differential equation (ODE) from the Gillespie algorithm [4] used for Ca^{2+} signaling in cellular tissues [2] to create the multi-carrier communication model and allow the analysis of molecular path loss and capacity for the joint use of IP_3 and Ca^{2+} . Our analysis follows the model presented next, being implemented in Python. Our results for end-to-end capacity and path loss show improvements when using combined IP_3 and Ca^{2+} molecules compared to the single-use of Ca^{2+} or IP_3 .

The paper proceeds as follows. Section II overviews the related works. Section III details the Ca^{2+} and IP_3 signaling-based molecular communication model. Section IV describes the evaluation method, and Section V discusses the results. Finally, Section VI concludes the paper.

II. RELATED WORKS

The signaling processes of human body cells can encode information based on the concentration of Ca^{2+} molecules, which is the pioneering work by Nakano and colleagues, where they presented the first end-to-end model of the Ca^{2+} signaling

communication system and the effectiveness of on-off-shift keying (OOK) using concentrations of molecules [5]. Thus, in [6], the authors investigated, through a set of simulation experiments, the communication capacity of the Ca^{2+} relay channel for a one-dimensional signaling system. That work was later extended by Barros *et al.* [2], who have modeled the in-body channel diversity for MC considering three distinct tissue types of astrocytes, epithelial, and muscular. They studied the capacity, delay, and intracellular interference communication behavior in a 3D tissue. In the same work, the authors also considered the simulation of the gap junctions and the noise. In [7], the authors presented a channel model for both intracellular and intercellular Ca^{2+} signaling and investigated the bit error probability for binary transmission, gain, and delay of Ca^{2+} waves traveling through a 1-D array of cells. In [8], the authors investigated different network topologies and their impact on calcium propagation.

Calcium is a very important molecule for the human body. This molecule controls or modulates different processes in the body, such as gene expression, neuroplasticity, growth, proliferation, differentiation, and cell death [9]. Many pathologies have been linked to abnormal $\text{IP}_3/\text{Ca}^{2+}$ molecules signaling as they affect the performance of the cells' natural communication processes (e.g., heart arrest, ischemia, Alzheimer's disease) [10]. In [8], the authors modeled how Alzheimer's disease affects astrocyte communications in terms of propagation, path loss, and delay. In [11], the researchers studied the safety of using Calcium Electroporation. In the treatment, a short electric pulse applied to the cell creates a temporary permeability in the cell membrane, which causes a high influx of intracellular Ca^{2+} resulting in cancer cell necrosis.

Ca^{2+} has already been used in adaptive communication algorithms for nanonetworks [12]. It can extend these to detect diseases such as Alzheimer's and others. However, these works, among others, have followed a single carrier approach, based only on Ca^{2+} molecule, which has advanced researches in molecular communications field, but it still requires performance improvements [2].

III. THE MULTI-CARRIER COMMUNICATION MODEL

This section details the multi-carrier model for the $\text{IP}_3/\text{Ca}^{2+}$ signaling process between the cells within astrocyte tissues. It describes the diffusion model that captures the temporal-spatial dynamics of intercellular signaling. The next subsections introduce the gap junction model that influences intercellular diffusion, describe the 3D model of the cellular tissue and discuss the stochastic model for the scheduling of reactions.

A. The $\text{IP}_3/\text{Ca}^{2+}$ Signaling

We consider a single-hop communication system composed of a transmitter, channel, and receiver. For the sake of exploring molecular diversity inside cellular tissues and providing richer mathematical analysis, we compare results for two different scenarios: (i) independence between IP_3 and Ca^{2+} channels; and (ii) dependence between these two channels following the natural $\text{IP}_3/\text{Ca}^{2+}$ information carriers

pathway (Fig. 1). The main entities in the communication system are transmitter and receiver nanomachines, and the channel, as described next.

A *transmitter nanomachine* is a synthetic cell able to encode data by molecule concentration. It follows an OOK modulation to transmit molecules in bit 1 periods (with a certain concentration) and not transmit molecules in bit 0 periods (concentration is zero). We use the $\text{IP}_3/\text{Ca}^{2+}$ cellular pathway for dependency, where their values are calculated as explained next in this section, or we employ pre-define values for independent transmission, otherwise.

The *channel* comprises the propagation of IP_3 and Ca^{2+} . It comprises the intracellular and intercellular signaling stages. Within the cell (intracellular), there are several chemical reactions to regulate Ca^{2+} concentration. Cell-to-cell communication (intercellular) occurs when the communicating gates (gap junctions) in the cells open. IP_3 or Ca^{2+} molecules propagate through the cytosol, i.e., the liquid that fills the cell cytoplasm.

The *receiver nanomachine* lies in a synthetic cell that receives the molecules and decodes the data transported by them. In the cell, there is a set of receptors responsible for the distribution and concentration of the received molecules. Decoding is based on the concentration value with a pre-define threshold detector. This process is ideal by merit of simplicity in this paper.

IP_3 or Ca^{2+} signaling in astrocytes supports molecular propagation, once these cells propagate intercellular Ca^{2+} molecules up to $100\mu\text{m}$ in response to IP_3 stimuli [13]. Intercellular signaling propagates Ca^{2+} molecules across the entire cellular tissue; whereas intracellular signaling can generate and/or amplify Ca^{2+} concentration in the cytosol. The mesostopic-type of diffusion of $\text{Ca}^{2+}/\text{IP}_3$ molecules is mediated by gap junctions that connect the cytosol of two cells.

We take as basis the work in [14] to describe Ca^{2+} oscillations in astrocyte cells. The model considers storage areas (pools); the variation of Ca^{2+} concentration in the cytosol (C_{cy}) (1); the variation of Ca^{2+} concentration in the endoplasmic reticulum (C_{er}) (2); and the variation of IP_3 concentration (IP) (3). We detail equations next.

$$\frac{dC_{cy}}{dt} = X_0 - k_0 C_{cy} + X_1 - X_2 + l_f, \quad (1)$$

$$\frac{dC_{er}}{dt} = X_2 - X_1 - l_f, \quad (2)$$

$$\frac{dIP}{dt} = X_3 - IP K_{deg}, \quad (3)$$

where

$$X_1 = 4M_3 \left(\frac{k_A^n C_{cy}^n}{(C_{cy}^n + k_A^n)(C_{cy}^n + k_I^n)} \right) \cdot \left(\frac{IP^m}{k_{IP}^m + IP^m} \right) \cdot l_f, \quad (4)$$

$$X_2 = M_2 \frac{C_{er}^2}{k_2^2 + C_{er}^2}, \quad (5)$$

$$X_3 = M_p \frac{C_{er}^2}{C_{er}^2 + k_p^2}. \quad (6)$$

X_0 is the concentration of Ca^{2+} in the flow from the extracellular space to the cytosol; and $k_0 C_{cy}$ is the baseline rate of Ca^{2+} in the outward flow from the cytosol to the extracellular space. l_f (i.e., $C_{cy} - C_{er}$) is the leak flow rate from the endoplasmic reticulum (ER) to the cytosol; and IP_{Kdeg} is the rate of IP_3 degeneration per second. The values for these parameters are based on experimental measurements presented in [15].

The term X_1 (4) models the Ca^{2+} flow rate from the ER to the cytosol under IP_3 stimulus. This mechanism directly affects the cytosolic concentration of Ca^{2+} . M_3 is the maximum value for the Ca^{2+} flux into cytosol; k_A and k_I relate, respectively, to the activation and inhibition factors for IP_3 ; k_2 and k_{IP} are threshold constants; and m and n are regular Hill coefficients. In molecular biology, Hill coefficients describe the level of cooperation between two biological processes (e.g., IP_3 activation and inhibition; Ca^{2+} inward and outward flux). A coefficient of 1 indicates complete independence; whereas a value greater than 1 indicates positive cooperation.

The Hill coefficient values employed in this study follow the same approach from [14], validated through experimental measurements. X_2 (5) models the efflux of Ca^{2+} from the sarco(endo)plasmic reticulum to the ER. M_2 is the maximum flux of Ca^{2+} in this process. Finally, X_3 (6) describes IP_3 generation by the Phosphoinositide phospholipase C (PLC) protein, where M_p is the maximum Ca^{2+} flux in this process, k the saturation constant for the cytosolic Ca^{2+} concentration, and p is a Hill coefficient.

B. Gap Junction Model

A single gap junction gate is formed by two cylindrical particles (connexons), one in each connecting cell (Fig. 2). Each connexon comprises six proteins, called connexins. We follow the stochastic model for gap junction behavior introduced in [3]. The model represents voltage-sensitive gap junctions with two states of conductance for each connexin: open meaning high conductance, and closed low conductance.

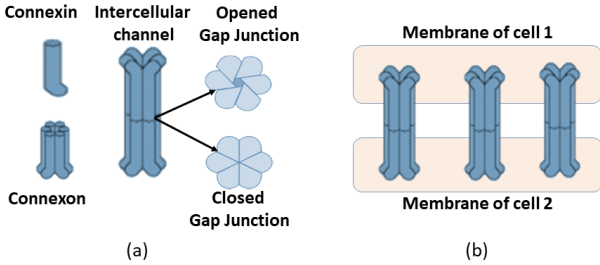


Fig. 2: (a) Individual gap junction view, and (b) two adjacent cells connected via gap junctions

We observe four possible combinations for all states of each connexon: (1) state g_1 – both connexon in the communicating cells are in a high conductance; (2) state g_2 – the first connexon is in a high conductance state and the second is in a low conductance; (3) state g_3 – first connexon is in a low conductance state and the second is in a high conductance; and (4) state g_4 – both connexons are in a low conductance.

However, once experimental validation of this model indicates a very low occurrence of the g_4 state [16], it is not considered in this work. Thus, the probabilities of the states should follow $P(g_1) + P(g_2) + P(g_3) = 1$. Moreover, g_1 , g_2 and g_3 are interrelated as follows:

$$\frac{dg_2}{dt} = \beta_1(\vartheta_j) \times g_1 - \xi_1(\vartheta_j) \times g_3, \quad (7)$$

$$\frac{dg_3}{dt} = \beta_2(\vartheta_j) \times g_1 - \xi_2(\vartheta_j) \times g_2, \quad (8)$$

The control of the gap junction permeability is mediated by the voltage difference (ϑ_j) between two adjacent cells membrane. ξ is the gate opening rate, and β the gate closing rate. The terms $\xi_1(\vartheta_j)$, $\xi_2(\vartheta_j)$, $\beta_1(\vartheta_j)$, $\beta_2(\vartheta_j)$ are defined as

$$\xi_1(\vartheta_j) = \lambda e^{-A\xi(\vartheta_j - \vartheta_0)}, \quad (9)$$

$$\xi_2(\vartheta_j) = \lambda e^{A\xi(\vartheta_j - \vartheta_0)}, \quad (10)$$

$$\beta_1(\vartheta_j) = \lambda e^{A\beta(\vartheta_j - \vartheta_0)}, \quad (11)$$

$$\beta_2(\vartheta_j) = \lambda e^{-A\beta(\vartheta_j - \vartheta_0)}, \quad (12)$$

where ϑ_0 is the voltage of the gap junction at which $\xi = \beta$. λ , $A\xi$ and $A\beta$ are constants indicating the responsiveness of a gap to its voltage.

C. Diffusion Model

The molecular diffusion (13) follows a model that captures the Spatio-temporal dynamics of intercellular signaling based on *mesoscopic diffusion* principles [6].

$$Z\Delta(i, j, k, n, m, l) = \frac{D\vartheta}{v} (|Z_{n,m,l} - Z_{i,j,k}|) \cdot \{P(g_1), P(g_2), P(g_3)\}, \quad (13)$$

where $Z\Delta(i, j, k, n, m, l)$ is the difference of molecular concentration between a pair of neighbors cells, being i, j, k the position of the transmitter cell; and n, m, l the position of the receiver cell. This value follows $\frac{D\vartheta}{v} (|Z_{n,m,l} - Z_{i,j,k}|)$, where D means the molecular diffusion coefficient for Ca^{2+} or IP_3 ; v is the astrocyte volume; $(|Z_{n,m,l} - Z_{i,j,k}|)$ is the difference in the concentration of molecules between transmitter and receiver cells. As we focus on the diffusion process of the Ca^{2+} or IP_3 molecules through the gap junctions, the probabilities $\{P(g_1), P(g_2), P(g_3)\}$ assume the open and close rates for each connexon, selected by the stochastic model and based on the states g_1 , g_2 and g_3 specified in Subsection III-B.

D. 3D Astrocyte Tissue Model and Stochastic Solver

We consider a cellular tissue with an area (A) composed of cells following a three-dimensional grid organization, as illustrated in Fig. 3. The indexes i, j and k indicate the position of a cell $c_{i,j,k}$ in the 3D grid, where i ranges from 1 to I ; j from 1 to J ; and k from 1 to K . In Fig. 3, P1 is the flow of IP_3 or Ca^{2+} from the cytosol into the extracellular space, and P2 the diffusion of Ca^{2+} from the ER to the cell cytosol. The model for connections between cells follows the study of the topologies found in astrocyte tissues [17].

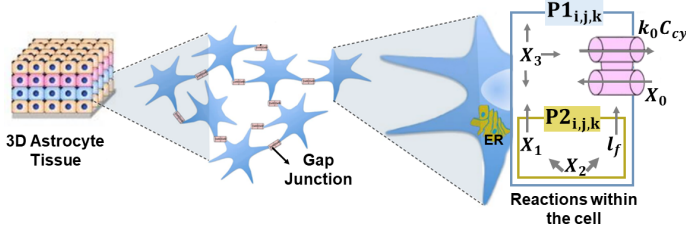


Fig. 3: 3D tissue with the intra-intercellular processes

The *Exact Stochastic Chemical Reaction-Diffusion* ODE solution from the Gillespie algorithm leads the dynamic intracellular/intercellular concentration. The ODE-based simulations produce accurate variability of the chemical reactions and serves to study noise effects caused by inherent stochastic behavior [6]. Our stochastic mathematical framework executes a Gillespie algorithm at each time step to select a random cell. It chooses a random internal reaction for the cell and schedules a time step (t) to that reaction. The execution of each reaction (R) follows a two-phases scheduling process: (i) selecting a reaction; and (ii) selecting a time step. Each reaction is allocated to a reaction constant (a_r). Considering that τ_0 is the sum of all a_r of R , the next reaction chosen (r_u) is given by (14).

$$r_u = \text{MAX} \left\{ \frac{a_{rj}}{\tau_0} = \frac{a_{rj}}{\sum_{j=1}^{|R|} a_{rj}} \right\}. \quad (14)$$

The reaction selection is based on the roulette wheel function, which is a biased process based on the reactions probability values. However, a roulette wheel selection (u) must satisfy (15).

$$\sum_{j=1}^{u-1} \frac{\tau_{rj}}{\tau_0} < \rho_1 \leq \sum_{j=1}^u \frac{\tau_{rj}}{\tau_0}, \quad (15)$$

which ρ_1 is a binary uniform random variable. We compute a time lapse (δ_t) at each time step (t) based on the initial τ_0 as

$$\tau_0 \cdot \delta_t = 1n \frac{1}{\rho_2}, \quad (16)$$

which ρ_2 is another binary uniform random variable. The end condition is $\sum_{t=0}^{|T|} \delta_t < t_0$, where T is the t set and t_0 is the pre-defined simulation time. Reactions are then time-varying variables based on the pool values changing, *i.e.*, according to the differential equations. A pre-defined reaction changing constant influences the set of values based on the positive or negative result of the reaction. Regarding to intercellular reactions, a_r is replaced by $Z\Delta$, as observed in (13).

IV. EVALUATION

This section follows two subsections that, respectively, present the analyses over end-to-end channel path loss and end-to-end information capacity of the multi-carrier molecular communication. Our analysis follows the model presented in Subsection III-A, which is implemented in Python. For simulations, we define parameter values based on experimental results from the literature [3], [14], [15], [18], [19]. Table I resumes the parameters values.

TABLE I: Simulation parameters

Variable	Value
C_a	$0.1 \mu M$
E_a	$1.5 \mu M$
I_a	$1.44 \mu M$
σ_0	$0.05 \mu M$
k_o	$0.5 s^{-1}$
k_f	$0.5 s^{-1}$
k_d	$0.08 s^{-1}$
ΣM_2	$15 \mu M/s$
Σ_p	$0.05 \mu M/s$
k_p	$0.3 \mu M$
n	2.02
k_{C1}	$0.15 \mu M$
k_{C2}	$0.15 \mu M$
ΣM_3	$40.0 s^{-1}$
m	2.02
D	$350 \mu m^2/s$
D_{IP_3}	$280 \mu m sec^{-2}$
λ	0.37
$\vartheta_j mV$	90
$\vartheta_0 mV$	60
$A\gamma(mV^{-1})$	0.008
$A\beta(mV^{-1})$	0.67

A. End-to-End Channel Path loss

In MC, molecules may not arrive at the receiver due to their diffusion direction probability in gap junction channels (13). We employ channel path loss (17) to study this behavior.

$$\Gamma(f) = 20 \log_{10} \left(\frac{\Gamma_T(f)}{\Gamma_{T_0}(f)} \right), \quad (17)$$

where $\Gamma_T(f)$ and $\Gamma_{T_0}(f)$ are the average peak and the initial peak of molecules, respectively, and (f) represents the frequency in hertz (Hz). Eq. 17 calculates the path loss for one individual molecule ($\Gamma^{IP_3}(f)$ or $\Gamma^{Ca^{2+}}(f)$). Hence, when using multi-carriers, we obtain the total path loss by $\Gamma_{total} = \Gamma^{Ca^{2+}} + \Gamma^{IP_3} + \gamma$, considering that the channel depends on both molecules and γ is a system noise. Then, by the sum of logs, Γ_{total} follows (18).

$$\Gamma_{total} = \left(20 \log_{10} \left(\frac{\Gamma_T^{Ca^{2+}}(f)}{\Gamma_{T_0}^{Ca^{2+}}(f)} \right) \right) + \left(20 \log_{10} \left(\frac{\Gamma_T^{IP_3}(f)}{\Gamma_{T_0}^{IP_3}(f)} \right) \right) + \gamma, \quad (18)$$

where $\Gamma_T^{Ca^{2+}}(f)$ and $\Gamma_T^{IP_3}(f)$ are the average peak concentration of Ca^{2+} and IP_3 , respectively; $\Gamma_{T_0}^{Ca^{2+}}(f)$ and $\Gamma_{T_0}^{IP_3}(f)$ are the initial peak of molecules for Ca^{2+} and IP_3 , respectively. γ is the system noise factor satisfying (19).

$$\gamma = \begin{cases} 0 & , \text{ when } IP_3 \perp Ca^{2+}, \\ N(\mu = 0, X_1^2)|_{dB} & , \text{ when } IP_3 \not\perp Ca^{2+}, \end{cases} \quad (19)$$

where \perp represents independence and $\not\perp$ no independence between the two types of molecules, respectively. $N(\mu, X_1^2)$ is a normal distribution, with mean μ and variance X_1^2 . Thereby, we check if the receiver after an eight-cells distance measures the same concentration as the sum of the two output values corresponding to a single molecule, transmitted independently without noise.

B. End-to-End Information Capacity

To investigate the end-to-end information capacity, we define the state transition probabilities for the receiver (Rx) and transmitter (Tx). For Tx, we consider: (i) the release of molecules ($x = x_1$) and (ii) silence ($x = x_0$). For Rx, we consider another two states: (i) active, i.e., when the number of received molecules changes a cell state ($y = y_1$), or (ii) inactive ($y = y_0$).

We assume a full synchronization of Rx and Tx. This assumption is common in the literature [6] and it is justified due to the high values for the employed discrete time-slots (Tb). Greater values for Tb enable a superior synchronization time when compared to other communication systems. The Shannon's entropy is a reliable measure of biological information capacity [20]. Also, the conditional entropy is defined based on the joint distribution, and the conditional distribution of x and y follows (20).

$$H(X|Y) = \sum_{x \in X} \sum_{y \in Y} p(x, y) \log_2 p(x|y), \quad (20)$$

where $Y = \{y_0, y_1\}$, and all the remaining probabilities are:

$$p(x) = p(x = x_0) + p(x = x_1) \quad (21)$$

$$p(y) = (p(y = y_0) + p(y = y_1)) * p(y|x) \quad (22)$$

$$p(y = y_0 | x = x_0) = 1 - p(y = y_1 | x = x_0) \quad (23)$$

$$p(y = y_0 | x = x_1) = 1 - p(y = y_1 | x = x_1) \quad (24)$$

To analyze the amount of transmitted data, we use the mutual information $I(X; Y)$. $p(x)$ and $p(y)$ are the probabilities of Tx and Rx states, respectively. Once the transmission period is relatively large and the effects of memory on the next bit transmission are reduced, we assume a memoryless channel. $I(X; Y)$ is based on the entropy $H(\cdot)$, and capacity follows (25). To calculate independence between the molecules, the probability of a bit transmission is the same for IP_3 and Ca^{2+} . We did not carry a detailed noise characterization and filtering from the information carrier, which implies that the capacity values tend to be close to a lower bound.

$$C(X; Y) = \max_{p(x)} I(X; Y) = \sum_{y \in Y} \sum_{x \in X} p(x) p(y | x) \log_2 \frac{p(y|x)}{p(y)}. \quad (25)$$

V. RESULTS

Fig. 4 shows the simulation results for Tx and Rx concentrations versus time. Results are for a $3 \times (3 \times l) \times (20 \times l)$ (μm) astrocyte tissue and l represents the length of each cell. In Figs. 4a and 4b, the Rx concentration is 500nM, the Tx initial concentration is 2×10^3 nM for both molecules and the distance is 8 cells. The natural oscillation frequency of the concentration levels in astrocytes is 0.1Hz. The amplitude of oscillations is $2.5 \mu\text{m}$ for IP_3 and $0.6 \mu\text{m}$ for Ca^{2+} measured by the maximum level of molecules. Based on the concentration levels alone, one observes different behaviors in Figs. 4a and 4b. A meaningful observation lies in how the IP_3 affects the intracellular Ca^{2+} signaling. IP_3 stimulation promotes an increase in Ca^{2+} concentration. IP_3 molecules

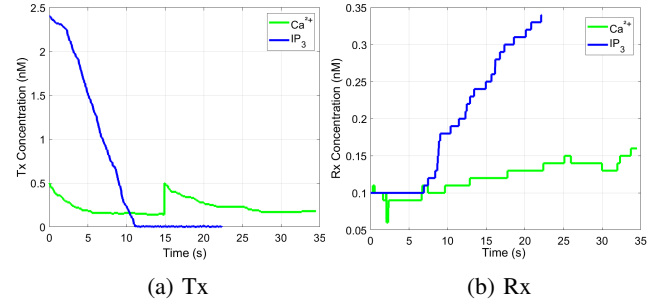


Fig. 4: Tx and Rx concentration

stimulate the Ca^{2+} production for a few more seconds, even when the last IP_3 molecule has already reached Rx.

In Fig. 5, results are for a $3 \times (3 \times l) \times (20 \times l)$ (μm) astrocyte tissue. For Ca^{2+} , the Tx concentration is 2×10^3 nM, and the Rx concentration is 1×10^5 nM. For IP_3 , the Tx initial concentration is 2×10^3 nM and the Rx concentration is of 6×10^5 nM. We increase the oscillation frequency to 1kHz to highlight the difference between the encoded bit 0 and 1, and its impact on capacity values. The pure Ca^{2+} propagation (Fig. 5) presents a higher path loss than IP_3 alone or when it is employed in conjunction with Ca^{2+} . As the distance between Tx and Rx increases, the path loss of the channel also increases for all combinations (Ca^{2+} , IP_3 , $IP_3 \perp Ca^{2+}$, $IP_3 \not\perp Ca^{2+}$), affecting performance. This result is explained by the diffusion mechanism in astrocyte cells (13), once their gap junctions are often in a high conductance state, allowing a high flow of molecules, which in turn, negatively affects propagation. Comparing Ca^{2+} and IP_3 path losses using single carrier and cell-distances ranging from 1 to 8, results show a smoother path loss for IP_3 when the evaluated distance comprise 2 to 6 cells and slight higher stability than Ca^{2+} along the entire path. When we use these molecules simultaneously (both in an independent or not independent way), we achieve a lower path loss in transmission, however an undesirable perturbation on the received molecular concentration may occur. This perturbation acts as a noise, represented by γ when $IP_3 \not\perp Ca^{2+}$. As shown in Fig. 5, this noise negatively influences how molecules propagate.

Fig. 6 presents results for the end-to-end capacity versus the distance (in number of cells) for a $3 \times (3 \times l) \times (20 \times l)$ (μm) astrocyte tissue. For Ca^{2+} , the Tx concentration is 2×10^3 nM, and Rx concentration is 1×10^5 nM. For IP_3 , the Tx initial concentration is 2×10^3 nM and the Rx concentration is of 6×10^5 nM. We increase the oscillation frequency to 1kHz to highlight the difference between the encoded bit 0 and 1, and its impact on capacity values. Rx activation relies on two variables: the concentration of received molecules by the external stimulus and the internal concentration of molecules. When the molecules distance themselves from Tx, their concentration reduces. Ca^{2+} is the most affected by distance. However, the diffusion process overcomes it, as well as the internal Ca^{2+} regeneration processes, due to the influence of IP_3 . This fast propagation leads to a low internal concentration of Ca^{2+} , while the high diffusion coefficient

REFERENCES

- [1] I. F. Akyildiz, M. Pierobon, S. Balasubramaniam, and Y. Koucheryavy, "The internet of bio-nano things," *IEEE Commun. Magazine*, vol. 53, no. 3, pp. 32–40, 2015.
- [2] M. T. Barros, S. Balasubramaniam, and B. Jennings, "Comparative end-to-end analysis of Ca^{2+} -signaling-based molecular communication in biological tissues," *IEEE Trans. on Communications*, vol. 63, no. 12, pp. 5128–5142, 2015.
- [3] S. Baigent, J. Stark, and A. Warner, "Modelling the effect of gap junction nonlinearities in systems of coupled cells," *J. of theoretical biology*, vol. 186, no. 2, pp. 223–239, 1997.
- [4] D. T. Gillespie, "Exact stochastic simulation of coupled chemical reactions," *The journal of physical chemistry*, vol. 81, no. 25, pp. 2340–2361, 1977.
- [5] T. Nakano, T. Suda, T. Koujin, T. Haraguchi, and Y. Hiraoka, "Molecular communication through gap junction channels: system design, experiments and modeling," in *IEEE Bionetics*, 2007, pp. 139–146.
- [6] T. Nakano and J.-Q. Liu, "Design and analysis of molecular relay channels: An information theoretic approach," *IEEE Trans. on NanoBio-science*, vol. 9, no. 3, pp. 213–221, 2010.
- [7] A. O. Bicen, I. F. Akyildiz, S. Balasubramaniam, and Y. Koucheryavy, "Linear channel modeling and error analysis for intra/inter-cellular Ca^{2+} molecular communication," *IEEE transactions on nanobioscience*, vol. 15, no. 5, pp. 488–498, 2016.
- [8] M. T. Barros, W. Silva, and C. D. M. Regis, "The multi-scale impact of the alzheimer's disease in the topology diversity of astrocytes molecular communications nanonetworks," *IEEE Access*, 2018.
- [9] B. Tandoğan and N. N. Ulusu, "Importance of calcium," *Turkish Journal of Medical Sciences*, vol. 35, no. 4, pp. 197–201, 2005.
- [10] E. Decrock, M. De Bock, N. Wang, A. K. Gadicherla, M. Bol, T. Delvaeye, P. Vandenabeele, M. Vincken, G. Bultynck, D. V. Krysko *et al.*, "IP₃, a small molecule with a powerful message," *Biochimica et Biophysica Acta (BBA)-Molecular Cell Research*, vol. 1833, no. 7, pp. 1772–1786, 2013.
- [11] C. C. Plaschke, J. Gehl, H. H. Johannesen, B. M. Fischer, A. Kjaer, A. F. Lomholt, and I. Wessel, "Calcium electroporation for recurrent head and neck cancer: A clinical phase i study," *Laryngoscope Investigative Otolaryngology*, vol. 4, no. 1, pp. 49–56, 2019.
- [12] M. T. Barros, S. Balasubramaniam, B. Jennings, and Y. Koucheryavy, "Adaptive transmission protocol for molecular communications in cellular tissues," in *Communications (ICC), 2014 IEEE International Conference on*. IEEE, 2014, pp. 3981–3986.
- [13] M. V. Khakh, Baljit S and Sofroniew, "Diversity of astrocyte functions and phenotypes in neural circuits," *Nature Neurosci.*, vol. 18, no. 7, p. 942, 2015.
- [14] M. Lavrentovich and S. Hemkin, "A mathematical model of spontaneous calcium (ii) oscillations in astrocytes," *J. of Theoretical Biology*, vol. 251, no. 4, pp. 553–560, 2008.
- [15] L. Venance, N. Stella, J. Glowinski, and C. Giaume, "Mechanism involved in initiation and propagation of receptor-induced intercellular calcium signaling in cultured rat astrocytes," *J. of Neuroscience*, vol. 17, no. 6, pp. 1981–1992, 1997.
- [16] F. F. Bukauskas, A. Bukauskiene, M. V. Bennett, and V. K. Verselis, "Gating properties of gap junction channels assembled from connexin43 and connexin43 fused with green fluorescent protein," *Biophysical journal*, vol. 81, no. 1, pp. 137–152, 2001.
- [17] J. Lallouette, M. De Pittà, E. Ben-Jacob, and H. Berry, "Sparse short-distance connections enhance calcium wave propagation in a 3d model of astrocyte networks," *Frontiers in Comp. Neurosci.*, vol. 8, p. 45, 2014.
- [18] A. Goldbeter, G. Dupont, and M. J. Berridge, "Minimal model for signal-induced Ca^{2+} oscillations and for their frequency encoding through protein phosphorylation," *Proceedings of the National Academy of Sciences*, vol. 87, no. 4, pp. 1461–1465, 1990.
- [19] T. Höfer, L. Venance, and C. Giaume, "Control and plasticity of intercellular calcium waves in astrocytes: a modeling approach," *Journal of Neuroscience*, vol. 22, no. 12, pp. 4850–4859, 2002.
- [20] P. Abshire and A. G. Andreou, "Capacity and energy cost of information in biological and silicon photoreceptors," *Proceedings of the IEEE*, vol. 89, no. 7, pp. 1052–1064, 2001.

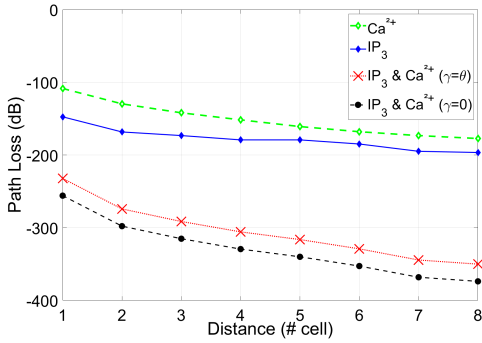


Fig. 5: End-to-end path loss as a function of the distance

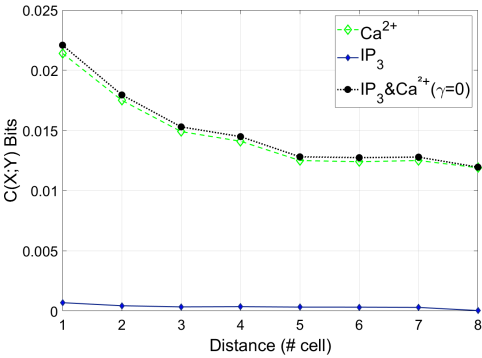


Fig. 6: End-to-end capacity as a function of the distance

causes a propagation that allows better performance over short distances. IP₃ presents low capacity values. However, it is stable for longer distance (seven cells). The use of both molecules improves performance.

Compared to the performance of pure Ca²⁺ molecules or pure IP₃, the results show that IP₃ has better performance in path loss and its propagation travels much faster. Besides that, the multi-carrier molecular communication using IP₃ and Ca²⁺ has overall superior performance. The cooperation between molecules reduces path loss, improves data propagation, and can be an alternative for data encoding and transmission.

VI. CONCLUSION

Molecular short range communication based on Ca²⁺ signaling in cellular tissues is a promising approach for in-vivo communication. This communication is necessary for the design of biological nanonetworks. Hence, this paper contributes with a multi-carrier MC model benefiting from molecular diversity in astrocyte tissue, a prominent type of cell that plays an important role to the neural system. The model allows to study the use of IP₃ and Ca²⁺ molecules as carriers and their behavior for end-to-end communication. Our results suggest that the cooperation between these two channels, i.e., IP₃ and Ca²⁺, can improve data encoding and transmission compared to their individual use (single carrier). As future work, we intend to explore the behavior of the multi-carrier model in different tissues as well as other molecular information carriers.